

## The Role of the Radial Electric Field, Reynolds Stress, and Zonal Flows in the L-H Transition in DIII-D

J.A. Boedo<sup>1</sup>, G.R. Tynan<sup>1</sup>, D.L. Rudakov<sup>1</sup>, Z. Yan<sup>2</sup>, G.R. McKee<sup>2</sup>, P. Manz<sup>1</sup>, L. Schmitz<sup>3</sup>, R.J. Groebner<sup>4</sup>, T.L. Rhodes<sup>3</sup>, G. Wang<sup>3</sup>, P. Diamond<sup>1</sup>, and the DIII-D Team<sup>4</sup>

<sup>1</sup>*University of California, San Diego, 9500 Gilman Dr., La Jolla, California 92093, USA*

<sup>2</sup>*University of Wisconsin-Madison, 1500 Engineering Dr., Madison, Wisconsin 53706, USA*

<sup>3</sup>*University of California Los Angeles, PO Box 957099, Los Angeles, California 90095, USA*

<sup>4</sup>*General Atomics, PO Box 85608, San Diego, California 92186-5608, USA*

Data from DIII-D provide a clear correlation between increases in  $E_r$ , i.e.  $E_r x B$ , poloidal flow, electrostatic Reynolds stress (RS) ( $\langle \tilde{v}_r \tilde{v}_\theta \rangle$ ) gradient, turbulence intensity, and poloidal velocity during limit cycle oscillations (LCOs) leading up to the H-mode transition. The RS and the  $E_r$  oscillations are slightly out of phase, consistent with causality, and they occur deeper than  $\sim 1$  cm inside the LCFS. The plasma was sampled at various times during the L-LCO-H evolution. The motivation for this work is that although we understand shear-decorrelation suppression of turbulence, detailed knowledge of how that shear spontaneously develops prior to the H-mode transition, and therefore scaling, is lacking.

The L-H transition [1] in tokamak plasmas is connected to velocity shear decorrelation of turbulence [2], but the detailed process is not fully understood, involving the evolution of self-organized, turbulence-generated, large scale flows [3]. Sheared zonal flows can be generated [4] nonlinearly by the gradient of the electrostatic RS by coupling energy from higher wavenumber fluctuations to low poloidal wavenumber flows. Thus this can be viewed as a predator-prey system where the energy in the turbulence feeds zonal flows (ZFs) that in turn suppress and decorrelate the turbulence [5,6].

We use discharge conditions that tether near the L-H transition, featuring slow (1–2 kHz) oscillations, dubbed limit cycle oscillations or LCOs, that are thought to be slowed-down L-H transitions dominated by the predator-prey dynamics between large scale flows and the turbulence, eventually followed by a second transition to a quiescent H-mode. This oscillating regime has been dubbed I-phase [5].

These plasmas are obtained in DIII-D with  $B_T = 2.1$  T,  $I_p = 1$  MA,  $n_e \sim 2.7 \times 10^{13}$ ,  $P_{in} \sim 500$  kW and keeping the LSN X-point at  $\sim 10$  cm or less from the floor [5] as shown in Fig. 1. The time evolution of the discharge is shown in Fig. 2, with the first vertical line marking the transition into the LCO regime at

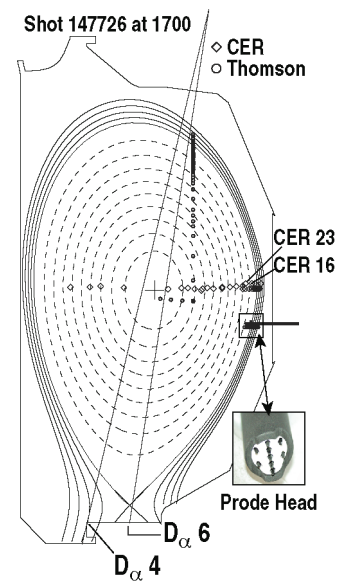


Fig. 1. LSN discharge magnetic topology showing the vertical  $D_\alpha$  chords, Thomson scattering chords, CER chords, tangential  $D_\alpha$  chords, and probe trajectory. Inset shows probe head.

~1590 ms and the second vertical line, at ~1850 ms the final transition into H-mode. Global measures of energy and particle confinement, such as line averaged  $T_e$  and  $N_e$  and stored energy, [Fig. 2(a–c)], start increasing after the first transition, and at an accelerated rate after the second transition into a quiet H-mode.

$D_\alpha$  measurements at the divertor [Fig. 2(d,e)] and Fig. 1] show an initial fast drop into the 2 kHz oscillations

for ~250 ms until the NBI input power is slightly increased [Fig. 2(c)], precipitating the second transition into H-mode. Plasma toroidal rotation and ion temperature near the edge [Fig. 2(f,g)], measured by charge exchange recombination (CER) on multiple chords (Fig. 1), increase upon entering the H-mode.

Probe measurements were performed using a 9-pin probe array, (Fig. 1, inset), that plunges for about 150 ms [Fig. 2(h–j)] and samples various plasma parameters. The current-drawing sensors (i.e. saturation current,  $I_{\text{sat}}$ ,  $T_e$  and flow measurements) were turned off in these experiments to reduce arcing, thus increasing probe plasma penetration. The focus is on obtaining multi-point plasma potential measurements  $V_{\text{pl}}$ , to deduce  $E_r$  and RS. In general (but not in this experiment), we measure  $T_e$  to estimate  $V_{\text{pl}}$  from the measurement of the floating potential,  $V_{\text{fl}}$ , obtained at various locations and combine them to get electric fields:

$$E_\theta = -\nabla_\theta V_{\text{pl}} = -\left( \frac{V_{\text{fl}}^{\theta+\delta\theta} - V_{\text{fl}}^\theta}{\delta\theta} \right) ,$$

which is a reasonable approximation since  $T_e$  is a flux surface quantity with negligible variation over 4 mm poloidally. Similarly, we approximate  $E_r$  based on:

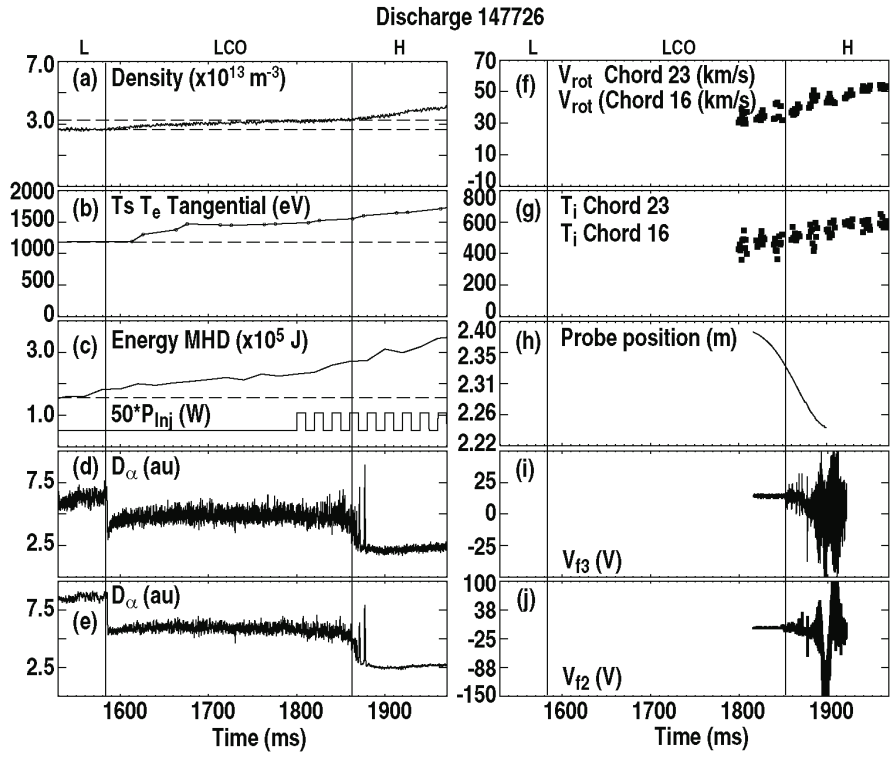


Fig. 2. Time evolution of the L-I-phase-H transition for discharge 147726, which starts at ~1590 ms, marked with the leftmost vertical bar; followed by the transition to H-mode at ~1870 ms and marked with the rightmost vertical bar. Evolution of (a) density, (b) central  $T_e$ , (c) energy content, (d,e)  $D_\alpha$  chords at the divertor, (f) toroidal rotation near the edge, and (g) ion temperature near the edge. The probe position during the plunge is shown in (h) and two floating potential traces in (i,j).

$$E_r = -\nabla_r V_{\text{pl}} = -\left(\frac{V_{\text{fl}}^{r+\partial r} - V_{\text{fl}}^r}{\partial r}\right) \approx -\left(\frac{V_{\text{fl}}^{r+\partial r} - V_{\text{fl}}^r}{\partial r} + 2.5 \times \frac{T_e^{r+\partial r} - T_e^r}{\partial r}\right) .$$

We will ignore the contribution of the  $T_e$  gradient to  $E_r$ , being much smaller in L-mode than in H-mode, and assume the floating potential gradient dominates the  $E_r$  gradient, at least at the deepest probe penetration. Time records 50–100  $\mu\text{s}$  long are used to calculate the fields and RMS quantities. Data is filtered below 1 kHz, low enough to eliminate low frequency components while keeping the 2 kHz oscillations of the zonal flow.

Timing/causality is shown in Fig. 3 over a time span of 2 ms by comparing  $D_\alpha$  at the divertor [Fig. 3(a)] with the floating potential,  $V_{\text{fl}}$  [Fig. 3(b)], and signals proportional to the radial and poloidal electric fields,  $E_r$  [Fig. 3(c)] and  $E_\theta$  [Fig. 3(d)]. The peaks in  $D_\alpha$ , a proxy for maximum radial transport, are preceded and accompanied by an increase in fluctuations in  $V_{\text{fl}}$  and  $E_\theta$  [circled area in Fig. 3(b)] that are then quenched by the increase in  $E_r$ , which reduces the transport, and the cycle starts again.

The  $E_r$  profile (shown in Fig. 4) was measured up to  $\sim 12$  mm inside the LCFS. The probe penetrates the discharge in L-mode (red) and during the dwell, the L-I transition (Fig. 2) occurs during the probe dwell in this discharge, resulting in a large increase in the average  $E_r$  from  $\sim 6 \times 10^3$  V/m to  $\sim 2 \times 10^4$  V/m while the LCOs, localized inside  $\sim 0.7$  cm, occur at  $\sim 2$  kHz frequency.

Direct probe measurements of RS,  $E_r$  (neglecting the  $T_e$  contribution as discussed earlier) and the fluctuations in  $E_\theta$ , a proxy for radial turbulent transport are shown in Fig. 5 together with an estimate (independent of  $E_r \times B$ ) of the plasma poloidal velocity using time delay estimate (TDE) techniques between two poloidally separated  $V_{\text{fl}}$  measurements with the assumption that the fluctuations are frozen to the plasma.

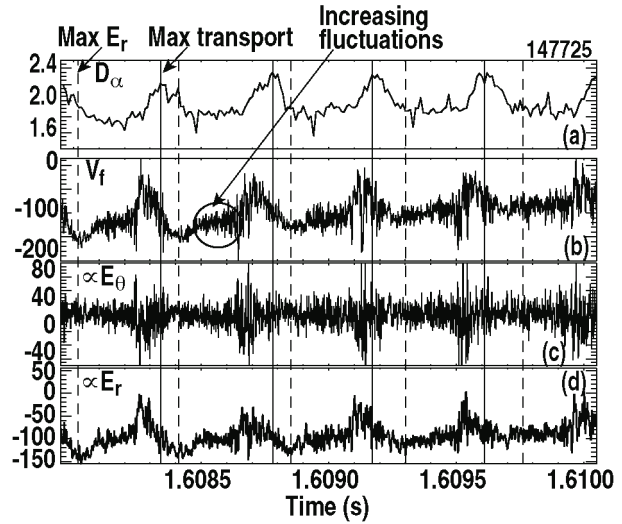


Fig. 3. Detail over a time period of 2 ms is shown: (a)  $D_\alpha$ , (b) floating potential, (c) proxy for  $E_\theta$  (not divided by  $d_\theta$ ), and (d) proxy for  $E_r$  (not divided by  $d_r$ ). Data is taken briefly after the L-I-phase transition and mainly during the probe dwell.

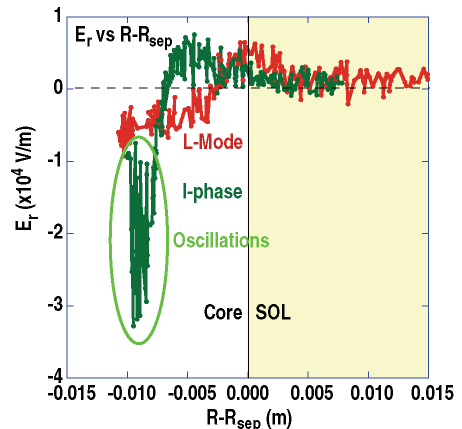


Fig. 4. Profile of approximate  $E_r$  from the probe. Probe is moving in during the L-mode and is at the dwell while the L-I-phase transition happens. The electric field oscillations are largest at about 1 cm inside the LCFS.

Causality of the predator-prey system can be examined by following the time evolution of all the terms during the L-I-phase transition as shown in [Fig. 5(a-d)]. A vertical dashed line is used as a guideline. The electric field [Fig. 5(a)] grows initially, reaching and  $E_r x B$  peak velocity (at  $B_T = 1.5$  T) is of the order of  $2 \times 10^4$  m/s and that compares well to the TDE-inferred peak velocity of  $\sim 0.5-1 \times 10^5$  m/s within the large scatter in the TDE calculation, due to the short records we are forced to use to properly resolve the LCOs.

The RS [Fig. 5(c)] grows and ebbs from  $0.2-1.5 \times 10^7$  m<sup>2</sup>s<sup>-2</sup> clearly *precedes* the peaking in  $E_r$  which is accompanied by a drop in  $E_\theta$ \_rms [Fig. 5(d)], indicating the fluctuations are suppressed by  $E_r$  and supporting causality and the predator-prey cycle.

Consistently with the reduction in the  $E_\theta$  fluctuations, global transport, reflected by  $D_\alpha$ , increases [Fig. 3(a,c)].

In conclusion, measurements on DIII-D show that during the LCOs, the RS profile steepens by a factor of 7, followed by a deepening of the  $E_r$  well and large sheared poloidal flows of the order of  $0.4-1 \times 10^5$  m/s that quench fluctuations and radial plasma transport. The RS profile then ebbs, followed by the shallowing of the  $E_r$  well, fluctuations grow and the process is repeated at roughly 2 kHz.

This work was supported in part by the US Department of Energy under DE-FG02-07ER54917, DE-FG02-89ER53296, DE-FG02-08ER54999, DE-FC02-04ER54698, and DE-FG02-08ER54984

- [1] F. Wagner, *et al.*, Phys. Rev. Lett. **49**, 1408 (1982).
- [2] H. Biglari, P. Diamond and P. Terry, Phys Fluids B **2**, 1 (1990).
- [3] C. Holland *et al.*, Phys. Plasmas **14**, 056112 (2007).
- [4] P.H. Diamond and Y.B. Kim. Phys. Fluids B **3**, 1626 (1991).
- [5] R.J. Colchin, *et al.*, Phys. Rev. Lett. **88**, 255002 (2002).
- [6] L. Schmitz, *et al.*, Phys. Rev. Lett. **108**, 155002 (2012).

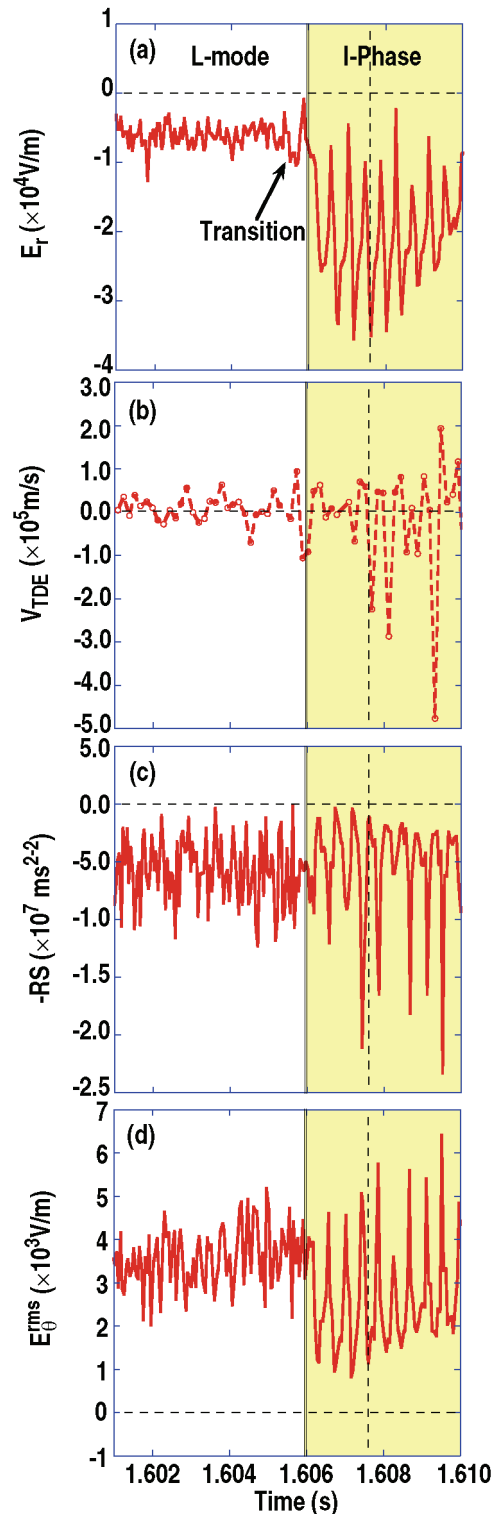


Fig. 5. The  $E_r$  oscillations (a) start as the plasma goes into the I-phase, transition indicated with a double vertical line at 1606 ms. Oscillations also shown with a vertical dashed line. (b) After the L-I-phase transition at  $\sim 1606$  ms, the  $E_r$  (top) and  $-RS$  (bottom) oscillations are clearly correlated, suggesting causality.